STATIC GRADIENT DAMAGE SIMULATIONS USING STABILIZED FINITE ELEMENTS

JERZY PAMIN, ADAM WOSATKO

Cracow University of Technology, Faculty of Civil Engineering, Kraków, Poland
e-mail: jpamin@L5.pk.edu.pl; awosatko@L5.pk.edu.pl

The hourglass control of two-field finite elements for the coupled problem of gradient damage is analyzed. For the equilibrium equations, stabilization is introduced according to the least-square method. For the additional averaging equation, three proposals of stabilization are considered, however only the γ operator method performs well. Attention is focused on the formulation, implementation and spectral analysis of four-noded elements in two-dimensional simulations. Basic benchmarks of a tensile bar with an imperfection and a beam in four-point bending are computed and discussed.

Key words: gradient damage, stabilized finite elements, localization of deformation

1. Introduction

It is common knowledge that if standard elements with reduced integration (RI) are used and improper hourglass modes have influence on the results, it can lead to a singularity of the assembled tangent operator for the finite element model and a stable numerical analysis becomes impossible. On the other hand, full integration (FI) can be inefficient, especially for large simulation problems. Furthermore, FI can cause a locking phenomenon in the mesh. Therefore, beside ideas like selective integration and $\bar{B}$ formulation, the concept of computations using one point integration with hourglass control is attractive for non-linear analysis.

The hourglass control, understood as mesh stabilization, was firstly applied in nonlinear FE analysis for the displacement field $\mathbf{u}$, see e.g. Belytschko *et al.* (1984). For two-field problems like the mixed $\mathbf{u} - p$ formulation, a mathematically motivated stabilization was introduced only for pressure p (Pastor *et al.*, 1997) or for both fields (Commend *et al.*, 2004). The hourglass control is also implemented in coupled problems, for example thermo-mechanical ones (Reese, 2003).

The issue addressed in this paper is the simulation of continuum damage. This involves, especially in quasi-brittle materials, the loss of well-possedness of the governing partial differential equations, hence regularization is necessary, cf. de Borst *et al.* (1993).

One of the successful regularized models of quasi-brittle failure is the gradient-enhanced damage formulation (Peerlings *et al.*, 1996). To solve this coupled problem of equilibrium and nonlocal averaging, two-field finite elements are used. Quadratic interpolation of the displacements and linear of the averaged strain can be introduced, hence a different number of degrees of freedom (dofs) at the corner and midside nodes is required. Although this interpolation option seems to be optimal, other possibilities can give stable results as shown in Pamin *et al.* (2003), since the analyzed problem is coupled rather than mixed. It is mentioned in Simone *et al.* (2004) that the so-called inf-sup condition does not have to be obeyed in this case. Oscillations which may appear for some secondary fields, for example the stress field, have a local character, i.e. occur only in zones of strong damage variation. Moreover, a linear interpolation of both fields is tempting due to the possibility of using one sampling point, of course with the hourglass control.

Especially in three-dimensional (3D) simulations, to reduce the computational cost and avoid locking phenomena, it would be advantageous to use eight-noded elements with linear interpolation of both the displacement vector field and the averaged strain field, and one-point Gaussian integration. Before attacking the 3D problem, this article covers the results obtained for the 2D four-noded gradient damage element with one-point reduced integration.

Variational and matrix equations for the gradient damage model are recollected in Section 2 in order to derive stabilization terms in Section 3. The analysis of the rank of stiffness matrix for the two-field four-noded FE is presented in Section 4. In next sections, we describe the results of two localized deformation tests, namely one-dimensional tension of a bar with an imperfection and four point bending of a concrete beam. Some final remarks are listed in Section 7.

2.   Variational and matrix equations for gradient damage

We begin our considerations from a recollection of the governing equations, weak forms and space discretization in gradient damage (Peerlings *et al.*, 1996). The whole set of small strain equations is as follows

$$\mathbf{L}^{\mathrm{T}}\boldsymbol{\sigma} + \mathbf{b} = \mathbf{0} \qquad\qquad \boldsymbol{\epsilon} = \mathbf{Lu} \qquad\qquad \boldsymbol{\sigma} = (1-\omega)\mathbf{E}\boldsymbol{\epsilon} \tag{2.1}$$

where $(2.1)_1$ are equilibrium equations, $(2.1)_2$ are kinematic equations and $(2.1)_3$ are constitutive relations for the scalar damage theory. In the above equations $\mathbf{L}$ is the matrix of differential operators, $\boldsymbol{\sigma}$ is the stress tensor in vector form, $\mathbf{b}$ is the body force vector, $\boldsymbol{\epsilon}$ is the strain tensor in vector form, $\mathbf{u}$ is the displacement vector, ω is the scalar damage parameter which grows from 0 to 1 and $\mathbf{E}$ is the elastic stiffness operator. The postulate of strain equivalence (Lemaitre, 1971) is adopted, so that the effective stress tensor $\hat{\boldsymbol{\sigma}} = \mathbf{E}\boldsymbol{\epsilon}$ as a fictitious undamaged counterpart of stresses is distinguished. We assume adequate boundary conditions. The well-known problem with mesh-dependent results is overcome by introducing the following differential equation for an averaged strain measure $\bar{\epsilon}$

$$\bar{\epsilon} - c\nabla^2\bar{\epsilon} = \tilde{\epsilon} \tag{2.2}$$

It is assumed that the homogeneous natural boundary condition $\mathbf{n}^{\mathrm{T}}\nabla\bar{\epsilon} = 0$ holds. A damage loading function $f^d = \bar{\epsilon} - \kappa^d = 0$ in strain space is used and standard loading-unloading conditions are applied. The damage ω grows with the history parameter κ^d. The gradient enhancement guarantees that the damage theory is nonlocal and the results become mesh-independent. The parameter $c > 0$ has a unit of length squared and it is connected with an internal length scale l of the material. The relation $c = l^2/2$ is derived for instance in Askes *et al.* (2000).

To solve the problem, apart from the approximation of displacements $\mathbf{u}$, we additionally discretize the averaged strain measure $\bar{\epsilon}$. The weak forms of equilibrium equations $(2.1)_1$ and averaging equation (2.2) are as follows

$$
\begin{aligned}
&\int_{\mathcal{B}} \delta\boldsymbol{\epsilon}^{\mathrm{T}}\boldsymbol{\sigma}\, dV = \int_{\mathcal{B}} \delta\mathbf{u}^{\mathrm{T}}\mathbf{b}\, dV + \int_{\partial\mathcal{B}} \delta\mathbf{u}^{\mathrm{T}}\mathbf{t}\, dS \\
&\int_{\mathcal{B}} \delta\bar{\epsilon}\bar{\epsilon}\, dV + \int_{\mathcal{B}} (\nabla\delta\bar{\epsilon})^{\mathrm{T}}c\nabla\bar{\epsilon}\, dV = \int_{\mathcal{B}} \delta\bar{\epsilon}\tilde{\epsilon}\, dV
\end{aligned}
\tag{2.3}
$$

Here $\mathbf{t}$ denotes tractions. Next we can apply the spatial interpolation of displacements $\mathbf{u} = \mathbf{Na}$ and the averaged strain measure $\bar{\epsilon} = \mathbf{h}^{\mathrm{T}}\mathbf{e}$ where $\mathbf{N}$ and $\mathbf{h}$ contain respective shape functions. Further, the strain field is approximated by the relation $\boldsymbol{\epsilon} = \mathbf{Ba}$ and the gradient of the averaged

strain by $\nabla \bar{\epsilon} = \mathbf{q}^{\mathrm{T}} \mathbf{e}$, where $\mathbf{B}$ and $\mathbf{q}$ contain derivatives of the respective shape functions. Now we obtain two variational equations

$$R_1(\delta \mathbf{a}, \mathbf{a}, \mathbf{e}) = \delta \mathbf{a}^{\mathrm{T}} \int_{\mathcal{B}} \mathbf{B}^{\mathrm{T}} \boldsymbol{\sigma}(\mathbf{a}, \mathbf{e}) \, dV - \delta \mathbf{a}^{\mathrm{T}} \int_{\mathcal{B}} \mathbf{N}^{\mathrm{T}} \mathbf{b} \, dV - \delta \mathbf{a}^{\mathrm{T}} \int_{\partial \mathcal{B}} \mathbf{N}^{\mathrm{T}} \mathbf{t} \, dS = 0$$

$$R_2(\mathbf{a}, \delta \mathbf{e}, \mathbf{e}) = \delta \mathbf{e}^{\mathrm{T}} \int_{\mathcal{B}} (\mathbf{h}\mathbf{h}^{\mathrm{T}} + c\mathbf{q}\mathbf{q}^{\mathrm{T}})\mathbf{e} \, dV - \delta \mathbf{e}^{\mathrm{T}} \int_{\mathcal{B}} \mathbf{h}\tilde{\epsilon}(\mathbf{a}) \, dV = 0 \tag{2.4}$$

After linearization of this gradient damage formulation, we introduce the following submatrices and vectors as in Peerlings *et al.* (1996)

$$\mathbf{K}_{aa} = \int_{\mathcal{B}} \mathbf{B}^{\mathrm{T}}(1 - \omega^i)\mathbf{E}\mathbf{B} \, dV \qquad\qquad \mathbf{K}_{ae} = -\int_{\mathcal{B}} \mathcal{G}^i \mathbf{B}^{\mathrm{T}} \hat{\boldsymbol{\sigma}}^i \mathbf{h}^{\mathrm{T}} \, dV$$

$$\mathbf{K}_{ea} = -\int_{\mathcal{B}} \mathbf{h}[\mathbf{s}^{\mathrm{T}}]^i \mathbf{B} \, dV \qquad\qquad \mathbf{K}_{ee} = \int_{\mathcal{B}} (\mathbf{h}\mathbf{h}^{\mathrm{T}} + c\mathbf{q}\mathbf{q}^{\mathrm{T}}) \, dV$$

$$\mathbf{f}_{ext}^{i+1} = \int_{\mathcal{B}} \mathbf{N}^{\mathrm{T}} \mathbf{b}^{i+1} \, dV + \int_{\partial \mathcal{B}} \mathbf{N}^{\mathrm{T}} \mathbf{t}^{i+1} \, dS \qquad \mathbf{f}_{int}^i = \int_{\mathcal{B}} \mathbf{B}^{\mathrm{T}} \boldsymbol{\sigma}^i \, dV \tag{2.5}$$

$$\mathbf{f}_\epsilon^i = \int_{\mathcal{B}} \mathbf{h}\tilde{\epsilon}^i \, dV \qquad\qquad \mathbf{f}_e^i = \mathbf{K}_{ee}\mathbf{e}^i$$

where

$$\mathcal{G} = \Big[\frac{\partial \omega}{\partial \kappa^d}\Big]\Big[\frac{\partial \kappa^d}{\partial \bar{\epsilon}}\Big] \qquad\qquad \mathbf{s}^{\mathrm{T}} = \frac{d\tilde{\epsilon}}{d\boldsymbol{\epsilon}}$$

Based on iteration i, the increments of the primary fields $d\mathbf{a}$ and $d\mathbf{e}$ are computed for iteration $i+1$

$$\begin{bmatrix} \mathbf{K}_{aa} & \mathbf{K}_{ae} \\ \mathbf{K}_{ea} & \mathbf{K}_{ee} \end{bmatrix} \begin{bmatrix} d\mathbf{a} \\ d\mathbf{e} \end{bmatrix} = \begin{bmatrix} \mathbf{f}_{ext}^{i+1} - \mathbf{f}_{int}^i \\ \mathbf{f}_\epsilon^i - \mathbf{f}_e^i \end{bmatrix} \tag{2.6}$$

The tangent operator in the above matrix equation is non-symmetric. The gradient damage model has been applied with success in the simulations of fracture in various materials, e.g. composites (Geers, 1997) or concrete (Geers *et al.*, 2000; Peerlings *et al.*, 1996). Its version refined by coupling to hardening plasticity (de Borst *et al.*, 1999) enables the incorporation of the physically observed irreversible strains.

3. Stabilization terms in variational equations

3.1. Stabilization of equilibrium equations

The mixed $\mathbf{u}-p$ formulation in Commend *et al.* (2004) is the starting point for the derivations below. It is possible to apply one integration point and control hourglass modes in the solution of equilibrium equations by the Galerkin least-square (GLS) method as in Zienkiewicz *et al.* (2005). A stabilization term is added to Eq. $(2.4)_1$

$$R_1(\delta \mathbf{a}, \mathbf{a}, \mathbf{e}) + R_1^{stab}(\delta \mathbf{a}, \mathbf{a}, \delta \mathbf{e}, \mathbf{e}) = 0 \tag{3.1}$$

The term R_1^{stab} can be defined according to the GLS method and for continuous fields is written as follows

$$R_1^{stab}(\delta \mathbf{u}, \mathbf{u}, \delta \bar{\epsilon}, \bar{\epsilon}) = \sum_{e=1}^{n_{el}} \int_{\mathcal{B}^e} [\mathbf{L}^{\mathrm{T}} \boldsymbol{\sigma}(\delta \mathbf{u}, \delta \bar{\epsilon})]^{\mathrm{T}} \boldsymbol{\chi}_1 [\mathbf{L}^{\mathrm{T}} \boldsymbol{\sigma}(\mathbf{u}, \bar{\epsilon}) + \mathbf{b}] \, dV \tag{3.2}$$

The stabilization scaling matrix $\boldsymbol{\chi}_1$ is assumed as

$$\boldsymbol{\chi}_1 = \frac{\chi h_e^2}{2G}\mathbf{I} \tag{3.3}$$

Here χ is an arbitrary, but possibly small value, h_e is a characteristic dimension of the finite element, for example its diagonal, and G is the shear modulus. A further explanation of the definition of $\boldsymbol{\chi}_1$ and the analysis of units are given in Commend *et al.* (2004).

The weighting part of the stabilization term for the equilibrium equations can be written in the following manner

$$\mathbf{P}_1(\delta\mathbf{u}, \delta\bar{\epsilon}) = \mathbf{L}^{\mathrm{T}}\boldsymbol{\sigma}(\delta\mathbf{u}, \delta\bar{\epsilon}) = \mathbf{L}^{\mathrm{T}}[(1 - \omega^i(\delta\bar{\epsilon}))\mathbf{E}\boldsymbol{\epsilon}(\delta\mathbf{u})] \tag{3.4}$$

As was done with the plastic part in Commend *et al.* (2004), to avoid the linearization of the damage part in Eq. (3.4), the damage contribution is omitted and only the elastic one kept. Further, instead of $\mathbf{P}_1(\delta\mathbf{u}, \delta\bar{\epsilon})$, its discrete counterpart $\mathbf{P}_1(\delta\mathbf{a})$ is introduced

$$\mathbf{P}_1(\delta\mathbf{a}) = \mathbf{L}^{\mathrm{T}}\mathbf{E}\mathbf{B}\delta\mathbf{a} = \mathbf{G}_a^e\delta\mathbf{a} \tag{3.5}$$

where an additional matrix is defined: $\mathbf{G}_a^e = \mathbf{L}^{\mathrm{T}}\mathbf{E}\mathbf{B}$.

The equilibrium is obtained in an iterative process and the stress is decomposed as $\boldsymbol{\sigma}_{i+1} = \boldsymbol{\sigma}_i + d\boldsymbol{\sigma}$. The definition of $\mathbf{R}_{\sigma,i+1}$ equal to $\mathbf{L}^{\mathrm{T}}\boldsymbol{\sigma}_{i+1}(\mathbf{u}, \bar{\epsilon})$ is introduced to obtain

$$\mathbf{R}_{\sigma,i+1} = \mathbf{L}^{\mathrm{T}}(\boldsymbol{\sigma}_i + d\boldsymbol{\sigma}) = \mathbf{R}_{\sigma,i} + d\mathbf{R}_\sigma \tag{3.6}$$

Constitutive equation $(2.1)_3$ of the damage theory can be rewritten in rate form

$$\dot{\boldsymbol{\sigma}} = (1 - \omega)\mathbf{E}\dot{\boldsymbol{\epsilon}} - \dot{\omega}\mathbf{E}\boldsymbol{\epsilon} \tag{3.7}$$

Further definitions are introduced: $\mathbf{E}_{aa} = (1 - \omega^i)\mathbf{E}$ and $\mathbf{E}_{ae} = -\mathcal{G}^i\mathbf{E}\boldsymbol{\epsilon}^i$, so that the following expression for $d\mathbf{R}_\sigma$ is derived

$$d\mathbf{R}_\sigma = \mathbf{L}^{\mathrm{T}}(\mathbf{E}_{aa}\mathbf{B}d\mathbf{a} + \mathbf{E}_{ae}\mathbf{h}^{\mathrm{T}}d\mathbf{e}) \tag{3.8}$$

Finally, we obtain the residuum

$$\mathbf{R}_{\sigma,i+1} = \mathbf{R}_{\sigma,i} + \mathbf{G}_a^d d\mathbf{a} + \mathbf{G}_e^d d\mathbf{e} \tag{3.9}$$

In the above relation, we have: $\mathbf{G}_a^d = \mathbf{L}^{\mathrm{T}}\mathbf{E}_{aa}\mathbf{B}$ and $\mathbf{G}_e^d = \mathbf{L}^{\mathrm{T}}\mathbf{E}_{ae}\mathbf{h}^{\mathrm{T}}$.

According to these derivations, the stabilization term (3.2) is equal to

$$R_1^{stab} = \sum_{e=1}^{n_{el}} \int_{\mathcal{B}^e} (\mathbf{G}_a^e\delta\mathbf{a})^{\mathrm{T}}\boldsymbol{\chi}_1(\mathbf{R}_{\sigma,i} + \mathbf{G}_a^d d\mathbf{a} + \mathbf{G}_e^d d\mathbf{e} + \mathbf{b})\, dV \tag{3.10}$$

The following submatrices and vectors are defined

$$\begin{aligned}
\widetilde{\mathbf{K}}_{aa} &= \int_{\mathcal{B}^e} (\mathbf{G}_a^e)^{\mathrm{T}}\boldsymbol{\chi}_1\mathbf{G}_a^d\, dV & \widetilde{\mathbf{K}}_{ae} &= \int_{\mathcal{B}^e} (\mathbf{G}_a^e)^{\mathrm{T}}\boldsymbol{\chi}_1\mathbf{G}_e^d\, dV \\
\widetilde{\mathbf{f}} &= \int_{\mathcal{B}^e} (\mathbf{G}_a^e)^{\mathrm{T}}\boldsymbol{\chi}_1(\mathbf{R}_{\sigma,i} + \mathbf{b})\, dV
\end{aligned} \tag{3.11}$$

3.2. Stabilization of averaging equation

In a similar manner, a stabilization term can be added to the averaging variational equation $(2.4)_2$

$$R_2(\mathbf{a}, \delta\mathbf{e}, \mathbf{e}) + R_2^{stab}(\delta\mathbf{a}, \mathbf{a}, \delta\mathbf{e}, \mathbf{e}) = 0 \tag{3.12}$$

In fact, in Commend *et al.* (2004) the sign before the term R_2 is changed to preserve the positive definiteness of the tangent operator. Here the sign remains positive. Apparently simple to perform, an analogical GLS method seems questionable for the averaging equation. After discretization, it turns out that for rectangular elements $\nabla^2 \mathbf{h}^{\mathrm{T}} = \mathbf{0}$, hence this method does not remove spurious singular modes. Clearly, in this case $\widetilde{\mathbf{K}}_{ee}$ is defined by the product $\mathbf{h}\mathbf{h}^{\mathrm{T}}$ like the original operator $\mathbf{K}_{ee}$, and the hourglass control fails. It is shown in detail in Wosatko (2008) and confirmed by a spectral analysis. Similarly, for the idea taken from Harari *et al.* (2002), where the gradient GLS method is considered, the stabilization operator $\widetilde{\mathbf{K}}_{ee}$ in the matrix equation arises as a result of multiplying matrix $\mathbf{q}$ and its transposition. An identical term is included in $\mathbf{K}_{ee}$, so that the hourglass control cannot work.

The third approach is a method based on the idea presented in Belytschko *et al.* (1984). If RI is used in a four-noded quadrilateral, the results are stabilized properly by means of the so-called $\boldsymbol{\gamma}$ operator method. Analogically to the analysis performed in Belytschko *et al.* (1984) for the Laplace equation, in this approach R_2^{stab} is taken into account as

$$R_2^{stab}(\delta\bar{\epsilon}, \bar{\epsilon}) = \sum_{e=1}^{n_{el}} \int_{\mathcal{B}^e} \delta\widetilde{g}^{\mathrm{T}} \chi_2 \widetilde{g}\, dV \tag{3.13}$$

where χ_2 is defined as follows

$$\chi_2 = \frac{\chi h_e^2}{2c} \tag{3.14}$$

This coefficient is calculated according to the dimensional analysis in Commend *et al.* (2004). The definitions of quantities χ and h_e are as previously, c is connected with the internal length parameter l. The variable $\widetilde{g}$ denotes a certain additional gradient connected with the averaged strain field. Discretization must be introduced in such a way that it satisfies the condition (Belytschko *et al.*, 1984)

$$\widetilde{g} = 0 \tag{3.15}$$

for any nodal values associated with a linear function $\bar{\epsilon}$. The rank of $\mathbf{K}_{ee}$, which is equal to 3 for RI (three positive eigenvalues), should be increased to 4 as is obtained for FI. Hence, after Belytschko *et al.* (1984) operator $\boldsymbol{\gamma}$ is adopted, which should not influence the linear fields

$$\boldsymbol{\gamma}^{\mathrm{T}} = a[\mathbf{t}_e - (\mathbf{t}_e^{\mathrm{T}}\mathbf{x}_e)\mathbf{q}_x - (\mathbf{t}_e^{\mathrm{T}}\mathbf{y}_e)\mathbf{q}_y] \tag{3.16}$$

where in the above relation additional element quantities must be defined (Belytschko *et al.*, 1984)

$$\mathbf{t}_e^{\mathrm{T}} = [-1, 1, -1, 1] \qquad \mathbf{x}_e^{\mathrm{T}} = [x_{e1}, x_{e2}, x_{e3}, x_{e4}] \qquad \mathbf{y}_e^{\mathrm{T}} = [y_{e1}, y_{e2}, y_{e3}, y_{e4}] \tag{3.17}$$

The parameter a can be equal to 1, because it is an arbitrary constant. The vector $\mathbf{t}_e$ constitutes in 2D a twisted form. The nodal coordinates are gathered in the vectors $\mathbf{x}_e$ and $\mathbf{y}_e$, the second index in their components refers to respective nodes. It should be emphasized that the derivatives of the shape functions $\mathbf{q}$ for the averaged strain field are separated in Eq. (3.16) to form $\mathbf{q}_x$

and $\mathbf{q}_y$. Analogically to the previous subsection, the discretization of the stabilization term R_2^{stab} is performed as follows

$$\widetilde{g} = \boldsymbol{\gamma}^{\mathrm{T}} \mathbf{e} \qquad\qquad \delta\widetilde{g} = \boldsymbol{\gamma}^{\mathrm{T}} \delta\mathbf{e} \tag{3.18}$$

where the discretized $\delta\widetilde{g}$ can be treated as the weighting part $\boldsymbol{P}_2(\delta\mathbf{e})$. The linearization of the residual can easily be derived

$$\widetilde{g}_{i+1} = \widetilde{g}_i + d\widetilde{g} = \widetilde{g}_i + \boldsymbol{\gamma}^{\mathrm{T}} d\mathbf{e} \tag{3.19}$$

Therefore, the term R_2^{stab} has the form

$$R_2^{stab} = \sum_{e=1}^{n_{el}} \int\limits_{\mathcal{B}^e} \boldsymbol{\gamma}\chi_2(\widetilde{g}_i + \boldsymbol{\gamma}^{\mathrm{T}} d\mathbf{e})\ dV \tag{3.20}$$

For the $\boldsymbol{\gamma}$ operator method, the additional matrix and vector are introduced

$$\widetilde{\mathbf{K}}_{ee} = \int\limits_{\mathcal{B}^e} \chi_2 \boldsymbol{\gamma}\boldsymbol{\gamma}^{\mathrm{T}}\ dV \qquad\qquad \widetilde{\mathbf{f}}_e = \int\limits_{\mathcal{B}^e} \chi_2 \boldsymbol{\gamma}\widetilde{g}_i\ dV \tag{3.21}$$

in order to obtain the final matrix equation to substitute Eq. (2.6)

$$\begin{bmatrix} \mathbf{K}_{aa} + \widetilde{\mathbf{K}}_{aa} & \mathbf{K}_{ae} + \widetilde{\mathbf{K}}_{ae} \\ \mathbf{K}_{ea} & \mathbf{K}_{ee} + \widetilde{\mathbf{K}}_{ee} \end{bmatrix} \begin{bmatrix} d\mathbf{a} \\ d\mathbf{e} \end{bmatrix} = \begin{bmatrix} \mathbf{f}_{ext} - \mathbf{f}_{int} - \widetilde{\mathbf{f}} \\ \mathbf{f}_\epsilon - \mathbf{f}_e - \widetilde{\mathbf{f}}_e \end{bmatrix} \tag{3.22}$$

The stabilization terms are needed in both variational equations, in order to ensure a proper quality of the FE and stable numerical results. It can be shown that an analogical approach to the stabilization of the equilibrium equations is equivalent to the one applied in the previous subsection in the GLS method. However, this equivalence is valid only for the four-noded FE. The GLS method seems to be more general, since the derivation is prepared for elements with an arbitrary number of nodes.

4.   Properties of four-noded element

In this section attention is focused on the description of the spectral analysis of a single FE, where RI (here one integration point) without or with stabilization is considered. The properties of elements including different types of interpolation and integration are described in detail in Wosatko (2008). The single FE is subjected to tension in one direction and two loading phases are considered: elasticity and damage. The computations of the eigenproblem for the tangent operator $\mathbf{K}$ in these phases are performed at the end of chosen incremental steps. The following material data are adopted (units are irrelevant and hence omitted): Young's modulus $E = 20000$, Poisson's ratio $\nu = 0.20$, the damage model with threshold $\kappa_o = 0.0001$ and linear softening where complete damage is for $\kappa_u = 0.002$. The internal length parameter c equals 1.

The signs of eigenvalues are shown in Table 1 for the whole tangent operator $\mathbf{K}$ and for particular submatrices $\mathbf{K}_{aa}$ and $\mathbf{K}_{ee}$. The accepted precision is equal to 1.0^{-10}, so that an absolute eigenvalue less than this limit is assumed to be zero. Obviously, three zero eigenvalues correspond to rigid motions of the element. However, when RI without any hourglass control is applied, more than three zero eigenvalues appear. They originate not only from $\mathbf{K}_{aa}$, but also one extra spurious zero eigenvalue comes from $\mathbf{K}_{ee}$, so altogether six such eigenvalues are present. A single element with RI and stabilization described in the previous section is then examined. The stabilization scaling factor χ is equal to 0.0001. The results in Table 1 show that in this case

Table 1. Signs of eigenvalues for FE with one integration point

(a) Without stabilization

	Elasticity			Damage		
sign	+	0	−	+	0	−
$\mathbf{K}_{aa}$	3	5	0	3	5	0
$\mathbf{K}_{ee}$	3	1	0	3	1	0
$\mathbf{K}$	6	6	0	5	6	1

(b) With stabilization, $\chi = 0.0001$

	Elasticity			Damage		
sign	+	0	−	+	0	−
$\mathbf{K}_{aa} + \widetilde{\mathbf{K}}_{aa}$	5	3	0	5	3	0
$\mathbf{K}_{ee} + \widetilde{\mathbf{K}}_{ee}$	4	0	0	4	0	0
$\mathbf{K} + \widetilde{\mathbf{K}}$	9	3	0	8	3	1

the stabilization according to Eq. (3.22) ensures a proper spectrum of eigenvalues. A negative eigenvalue for $\mathbf{K}$ appears after the peak during the damage progress and is related to softening in the material model.

The analysis of eigenforms for all loading phases and considered cases can be found in Wosatko (2008). It is emphasized that the tangent operator $\mathbf{K}$ is non-symmetric, so imaginary parts of components of eigenvectors in the spectral analysis are admitted. For RI without stabilization in the damage phase, non-zero values arise in one eigenvector for both subspaces: displacement and averaged strain fields. The coupling in the formulation is visible for this mode and it corresponds to the negative eigenvalue. Six zero eigenvalues of operator $\mathbf{K}$ are separated in such a way that five of them originate from the part connected with submatrix $\mathbf{K}_{aa}$ and the last one – from submatrix $\mathbf{K}_{ee}$.

When the stabilization is adopted, we observe that the spurious eigenforms for the displacement field vanish. Two in-plane bending modes are related to the double eigenvalue equal to 8.2512. It is connected with the stabilization of equilibrium equations. The coupling of variational equations can also be noticed for two eigenforms. Three eigenforms with zero eigenvalues correctly correspond to the combination of rigid motions. The eigenform with the non-zero eigenvalue and twisted mode in the averaged strain space proves that the stabilization of the averaging equation is active. Moreover, the second field is stabilized by the $\boldsymbol{\gamma}$ method, where operator $\boldsymbol{\gamma}$ for a rectangular element is reduced to the twist vector $\mathbf{t}_e$.

5. Bar with imperfection

The simulation of uniaxial tension for a bar with an imperfection in the middle is the most basic localization test in physically nonlinear mechanics. Here the length of the bar is equal to 100 mm and discretization introduces 20 FEs. Plane stress is assumed with both the width and thickness equal to 5 mm. The material data are as follows: Young's modulus E is 20000 MPa, Poisson's ratio equals zero. For gradient damage, the internal length parameter is adopted $c = 4\,\text{mm}^2$ ($l = 2.83\,\text{mm}$) and the damage threshold is $\kappa_o = 0.0001$. The threshold is reduced by 10% in the middle of the bar to introduce imperfection. The damage growth equivalent to linear softening is employed and the ultimate value $\kappa_u = 0.0125$. The load control and the arc length method are used. Two integration schemes are confronted: full integration (FI) and reduced integration (RI) with stabilization according to Eq. (3.22) and the coefficient $\chi = 0.000001$.

Generally, if FI is employed for the second or both discretized fields, the relation between elongation $u(L)$ and the stress σ is like for a slightly stiffer bar. The diagram for FI, presented in Table 2, ends before the stress approaches zero, but it is connected with the fact that the damage history parameter reaches the ultimate value κ_u and an unwanted change of the stiffness or unloading is obtained. Two types of integration are compared in Table 2. Four or five characteristic steps are chosen according to the figures placed at the top of the table. A completely different number of active integration points (ips) is observed as a consequence of the adopted

integration in an FE. It is confirmed that the solution exhibits quadratic convergence in every step for both integration cases.

Table 2. Convergence study – bar with imperfection. Two types of integration

Type	FI: $2 \times 2 = 4$ ips		RI + stabilization: 1 ips	
Step No.	Relative energy norm	Active ips	Relative energy norm	Active ips
2	1.000000000000000E+00	8	1.000000000000000E+00	2
	5.32118744198386E+02	8	5.763488320259804E+02	2
	2.534990264376641E–04	8	6.048211715158885E–04	2
	1.770959355358748E–10	8	1.304413629483436E–09	2
	8.617827040306284E–23	8	6.008164724480290E–21	2
22	1.000000000000000E+00	40	1.000000000000000E+00	8
	–9.779478750996960E–06	40	–3.149860222058139E–04	8
	1.548406070066814E–10	40	–7.542830989034233E–12	8
	3.871666510054424E–11	40	–1.885723762863035E–12	8
	1.260922539766909E–19	40	4.655693122775198E–24	8
77	1.000000000000000E+00	12	1.000000000000000E+00	4
	–6.737739431886433E–02	12	–8.738447627994261E–02	4
	–1.936878713736846E–19	12	1.595955486024598E–16	4
			–3.543616722096119E–27	4
122	1.000000000000000E+00	12	1.000000000000000E+00	4
	–8.424036872173256E–02	12	–5.664603859365940E–01	4
	–3.265570463637080E–20	12	6.614336369593637E–19	4
143			1.000000000000000E+00	4
			–6.109566557762603E–01	4
			3.162731767832675E–19	4

The averaged strain and damage distributions just after the peak and at the final state are shown in Figs. 1 and 2, respectively. Both the variables have similar distributions just after the peak load and also in the final state.

(a) Averaged strain, after peak

(b) Damage, after peak

(c) Averaged strain, final state

(c) Damage, final state
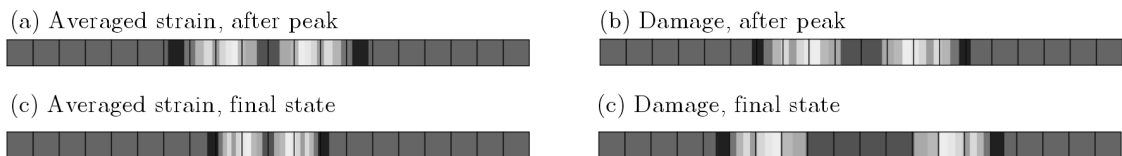
Fig. 1. Results for bar with imperfection – elements with FI

(a) Averaged strain, after peak

(b) Damage, after peak

(c) Averaged strain, final state

(d) Damage, final state
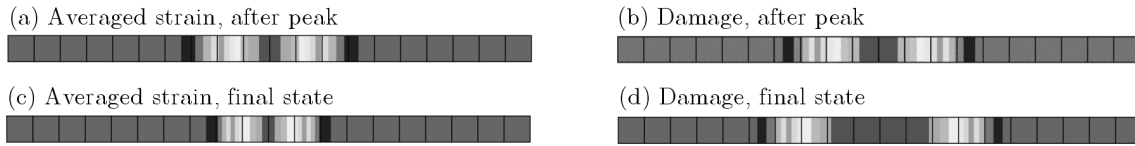
Fig. 2. Results for bar with imperfection – elements with RI and stabilization

6. Four point bending in concrete beam

The four-point bending of a concrete beam is simulated. This benchmark is based on a reinforced concrete beam, which was subjected to dynamic loading in experiments carried out by Eibl *et al.*(1994) and then computed e.g. in Sluys (1994) and Dubé *et al.* (1996). The results of simulations for the RC beam using the gradient damage model were presented in Wosatko *et al.* (2006), and now we limit our analysis to the verification of two different combinations of integration schemes as in the previous section. The geometry data are depicted in Fig. 3. Two supports are introduced at the bottom of the beam, while the loading is imposed at two points at the top. Plane stress conditions are assumed. The material data are: Young's modulus $E = 32940\,\mathrm{MPa}$, Poisson's ratio $\nu_c = 0.2$ and damage threshold $\kappa_o = 95.6 \times 10^{-6}$. In the experiment, concrete was additionally reinforced by Dramix fibers (1.2% volume). The modified von Mises definition is employed as the damage loading function (see de Vree *et al.*, 1995). The damage growth function asymptotically increases but never reaches 1 according to exponential softening (Mazars and Pijaudier-Cabot, 1989), the material ductility parameter η is equal to 350 and $\alpha = 0.96$, which is responsible for residual stresses. Based on the results presented in Wosatko *et al.* (2006), the internal length $l = 16\,\mathrm{mm}$ is adopted. Computations are performed for three FE meshes, namely: coarse – 56×8, medium – 112×16 and fine – 168×24 elements. Displacement control is used. If one-point integration and stabilization is applied, the scaling factor χ is equal to 0.0001.
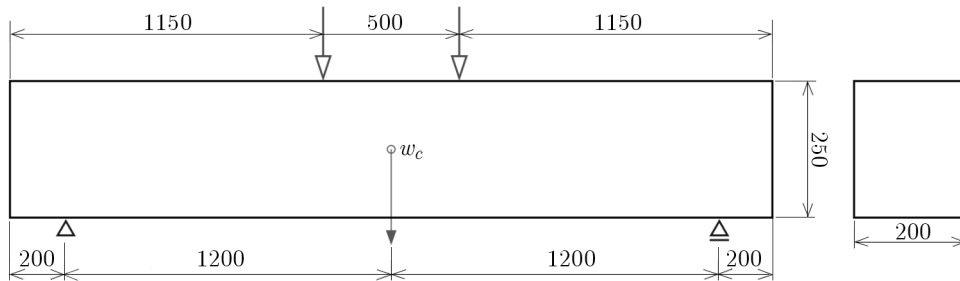
Fig. 3. Four-point bending in concrete beam

From the comparison of diagrams in Fig. 4, the general tendency is observed for RI and stabilized FEs that a slightly smaller load carrying capacity is obtained than for the computations with FI. As expected for RI, the simulated behaviour gives a response as for a slightly less stiff beam. The general character of diagrams does not differ significantly. The diagrams for the fine mesh are the nearest to each other.

From Fig. 5 with the deformations of the meshes and Fig. 6 with the corresponding contour plots of the averaged strain measure, it is noticed that two zones of localization are simulated. An exception occurs for the case with coarse mesh and FI. Of course these zones can be associated with cracking of the beam. It is also confirmed in Figs. 5a and 6a that, among the calculated cases, the solution for the coarse mesh and full integration leads to the stiffest model. However,
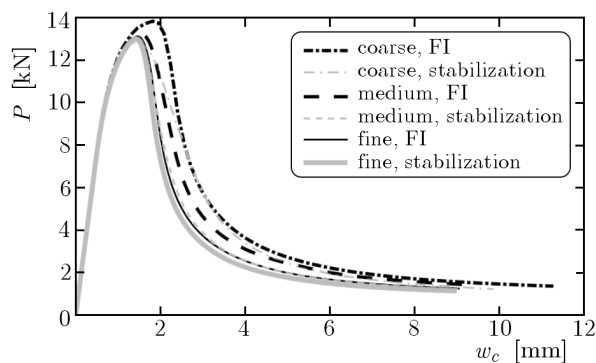
Fig. 4. Load-deflection diagrams – different meshes and integration schemes

(a) Coarse mesh, full integration FI

(b) Coarse mesh, stabilization

(c) Medium mesh, full integration FI

(d) Medium mesh, stabilization

(e) Fine mesh, full integration FI

(f) Fine mesh, stabilization
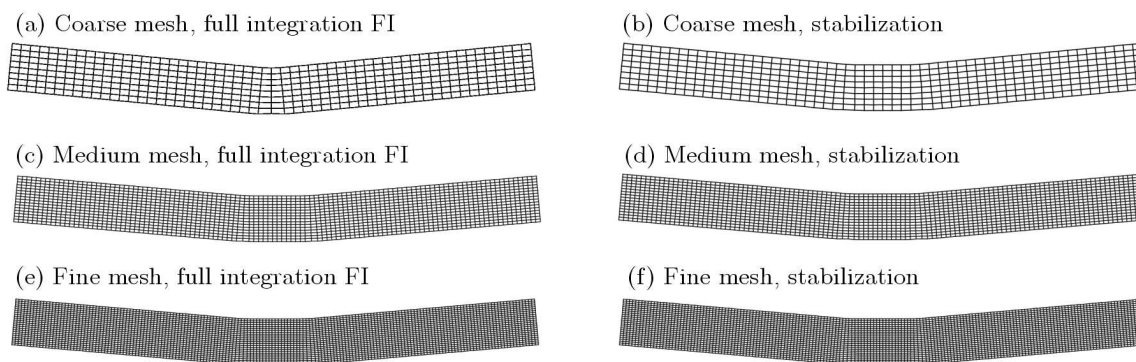
Fig. 5. Deformation – influence of meshes and integration schemes

(a) Coarse mesh, full integration FI

(b) Coarse mesh, stabilization

(c) Medium mesh, full integration FI

(d) Medium mesh, stabilization

(e) Fine mesh, full integration FI

(f) Fine mesh, stabilization
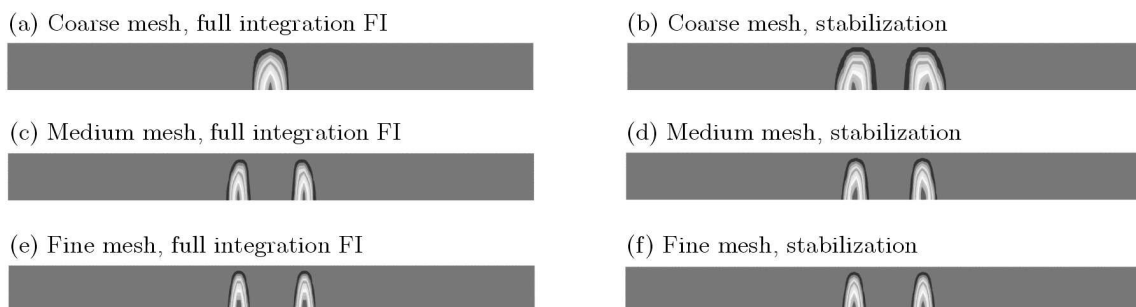
Fig. 6. Averaged strain distribution – different meshes and integration schemes

according to the plastic hinges theory in bars, both forms of deformation, both crack patterns and hence one or two localization zones are admissible. Moreover, mesh-independent results are obtained for both integration schemes.

The last aspect of our analysis is the verification of the impact of the parameter χ on the obtained results. A proper value of the scaling factor is necessary to ensure a numerically stable response as mentioned in Section 3. On the other hand, the parameter should have a possibly small value. In previous computations in this example, χ equals 0.0001. Now we vary this value from the smallest 0.00000001 up to the largest 1.0 with multiplier 100 for each case.

The diagram in Fig. 7 and the deformation of the mesh in Fig. 8a show that a too small value of the scaling factor does not guarantee proper stabilization for one-point integration in FE and even hourglass patterns can appear. For the case with a large value, for example $\chi = 1.0$, the response is considerably stiffer, although two localization zones are still obtained.
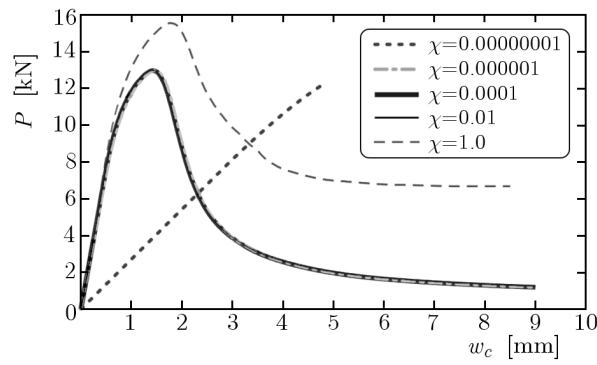
Fig. 7. Load-deflection diagrams – influence of scaling factor χ for medium mesh

(a) χ=0.00000001

(b) χ=1.0

Fig. 8. Deformation for medium mesh – influence of scaling factor χ

7. Conclusions

When one-point reduced integration is applied in the four-noded FE then, for effective computations, a stabilization must be introduced in the formulation.

Moreover, as shown in Section 3, for gradient damage finite elements with linear interpolation and one integration point, hourglass control must be incorporated for both primary fields. In the spectral analysis with RI additional spurious eigenforms, which appear for the displacements and for the averaged strain measure, confirm that hourglass control (mesh-stabilization) is needed. The stabilization terms are derived using the GLS method for the equilibrium equations and the γ operator method for the averaging equation. This is because, as discussed in Section 3.2, neither the GLS nor the gradient GLS methods provide effective stabilization for the latter equation.

The analysis of a bar with an imperfection shows that the solution guarantees quadratic convergence when RI with stabilization is used. The reduced integration results in a slightly less stiff response of the model, which is consistent with what is known about the influence of integration quadrature on FE results. This is also observed for the simulation of a concrete beam in four-point bending. The influence of the stabilization scaling factor χ on the results is examined.

The research is planned to be continued towards a 3D formulation. The elaboration of the formulation with an effective stabilization for the 3D brick element requires further research, but the derivation in Section 3 can constitute its initial point. It turns out that for 2D simulations the computation cost reduction in comparison to full integration is smaller than expected, but the implementation in FEAP package (Taylor, 2001) has not been optimized for the execution time. It is expected that the gain in 3D simulations would be much larger, even though the solver efficiency is then the main computation cost factor.

References

1. ASKES H., PAMIN J., DE BORST R., 2000, Dispersion analysis and element-free Galerkin solutions of second- and fourth-order gradient-enhanced damage models, *Int. J. Numer. Meth. Engng*, **49**, 811-832

2. BELYTSCHKO T., ONG J.S.-J., LIU W.K., KENNEDY J.M., 1984, Hourglass control in linear and nonlinear problems, *Comput. Methods Appl. Mech. Engrg.*, **43**, 251-276

3. COMMEND S., TRUTY A., ZIMMERMANN T., 2004, Stabilized finite elements applied to elasto-plasticity: I. mixed displacement-pressure fromulation, *Comput. Methods Appl. Mech. Engrg.*, **193**, 3559-3586

4. DE BORST R., PAMIN J., GEERS M.G.D., 1999, On coupled gradient-dependent plasticity and damage theories with a view to localization analysis, *Eur. J. Mech. A/Solids*, **18**, 6, 939-962

5. DE BORST R., SLUYS L.J., MÜHLHAUS H.-B., PAMIN J., 1993, Fundamental issues in finite element analyses of localization of deformation, *Eng. Comput.*, **10**, 99-121

6. DE VREE J.H.P., BREKELMANS W.A.M., VAN GILS M.A.J., 1995, Comparison of nonlocal approaches in continuum damage mechanics, *Comput. and Struct.*, **55**, 4, 581-588

7. DUBÉ J.-F., PIJAUDIER-CABOT G., LA BORDERIE CH., 1996, Rate dependent damage model for concrete in dynamics, *J. of Engng. Mech.*, *122*, 10, 939-947

8. EIBL J., BISCHOFF P.H., LOHRMANN G., 1994, Failure mechanics of fibre-reinforced concrete and pre-damaged structures: dynamic loading conditions, Technical Report BRITE/EURAM P-89-3275, Univ. of Karlsruhe, Karlsruhe, Germany

9. GEERS M.G.D., 1997, *Experimental Analysis and Computational Modelling of Damage and Fracture*, Ph.D. dissertation, Eindhoven University of Technology, Eindhoven

10. GEERS M.G.D., DE BORST R., PEERLINGS R.H.J., 2000, Damage and crack modeling in single-edge and double-edge notched concrete beams, *Eng. Fract. Mech.*, **65**, 247-261

11. HARARI I., FREY S., FRANCA L.P., 2002, A note on a recent study of stabilized finite element computations for heat conduction, *Computational Mechanics*, **28**, 63-65

12. LEMAITRE J., 1971, Evaluation of dissipation and damage in metals, [In:] *Proc. I.C.M.*, vol. 1, Kyoto, Japan

13. MAZARS J., PIJAUDIER-CABOT G., 1989, Continuum damage theory – application to concrete, *ASCE J. Eng. Mech.*, **115**, 345-365

14. PAMIN J., WOSATKO A., WINNICKI A., 2003, Two- and three-dimensional gradient damage-plasticity simulations of cracking in concrete, [In:] N. Bićanić et al. (Edit.), *Proc. EURO-C 2003 Int. Conf. Computational Modelling of Concrete Structures*, Rotterdam/Brookfield, A.A. Balkema, 325-334,

15. PASTOR M., QUECEDO M., ZIENKIEWICZ O.C., 1997, A mixed displacement-pressure formulation for numerical analysis of plastic failure, *Comput. and Struct.*, **62**, 1, 13-23

16. PEERLINGS R.H.J., DE BORST R., BREKELMANS W.A.M., DE VREE J.H.P., 1996, Gradient-enhanced damage for quasi-brittle materials, *Int. J. Numer. Meth. Engng*, **39**, 3391-3403

17. PEERLINGS R.H.J., DE BORST R., BREKELMANS W.A.M., GEERS M.G.D., 1998, Gradient-enhanced damage modelling of concrete fracture, *Mech. Cohes.-frict. Mater.*, **3**, 323-342

18. REESE S., 2003, On a consistent hourglass stabilization technique to treat large inelastic deformations and thermo-mechanical coupling in plane stress problems, *Int. J. Numer. Meth. Engng*, **57**, 1095-1127

19. SIMONE A., ASKES H., PEERLINGS R.H.J., SLUYS L.J., 2003, Interpolation requirements for implicit gradient-enhanced continuum damage models, *Communications in Numerical Methods in Engineering*, **19**, 563-572 (see also Simone *et al.*, 2004)

20. SIMONE A., ASKES H., PEERLINGS R.H.J., SLUYS L.J., 2004, Corrigendum 'Interpolation rquirements for implicit gradient-enhanced continuum damage models', *Communications in Numerical Methods in Engineering*, **20**, 163-165

21. SLUYS L.J., 1994, Dynamic failure in reinforced concrete structures, [In:] G.M.A. Kusters and M.A.N. Hendriks (Edit.), *DIANA Computational Mechanics '94*, 193-203, Dordrecht, Kluwer Acadamic Publishers

22. TAYLOR R.L., 2001, FEAP – A Finite Element Analysis Program, Version 7.4, User manual, University of California at Berkeley, Berkeley

23. WOSATKO A., 2008, *Finite-Element Analysis of Cracking in Concrete Using Gradient Damage-Plasticity*, Ph.D. dissertation, Cracow University of Technology, Cracow

24. WOSATKO A., PAMIN J., WINNICKI A., 2006, Gradient damage in simulations of behaviour of RC bars and beams under static and impact loading, *Archives of Civil Engineering*, **52**, 1, 455-477

25. ZIENKIEWICZ O.C., TAYLOR R.L., ZHU J.Z., 2005, *The Finite Element Method: Its Basis and Fundamentals*, Elsevier Butterworth-Heinemann, sixth ed.

Gradientowy model do statycznych symulacji uszkodzenia przy użyciu elementów skończonych ze stabilizacją

Streszczenie

W artykule przedstawiono dwupolowe elementy skończone z kontrolą pasożytniczych form deformacji, sformułowane dla sprzężonego problemu gradientowej mechaniki uszkodzenia. Zastosowano stabilizację równań równowagi zgodnie z metodą najmniejszych kwadratów. Rozpatrzono trzy warianty stabilizacji dodatkowego równania uśredniającego, z których tylko metoda wykorzystująca operator γ jest skuteczna. Uwaga została skupiona na wyprowadzeniu, implementacji i analizie spektralnej czterowęzłowego elementu do symulacji dwuwymiarowych. Przedyskutowano wyniki uzyskane dla podstawowych testów rozciąganego pręta z imperfekcją i belki czteropunktowo zginanej.